

Accepted Manuscript

Applicability of [^{11}C]PIB micro-PET imaging for *in vivo* follow-up of anti-amyloid treatment effects in APP23 mouse model

Anniina Snellman, Johanna Rokka, Francisco R. Lopez-Picon, Semi Helin, Francesca Re, Eliisa Löyttyniemi, Rea Pihlaja, Gianluigi Forloni, Mario Salmona, Massimo Masserini, Olof Solin, Juha O. Rinne, Merja Haaparanta-Solin

PII: S0197-4580(17)30163-X

DOI: [10.1016/j.neurobiolaging.2017.05.008](https://doi.org/10.1016/j.neurobiolaging.2017.05.008)

Reference: NBA 9930

To appear in: *Neurobiology of Aging*

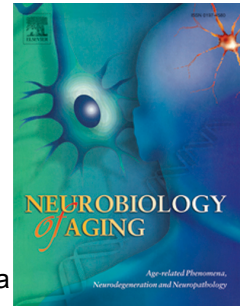
Received Date: 3 March 2017

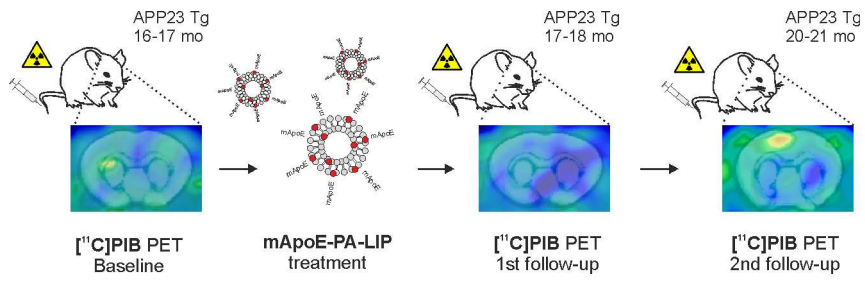
Revised Date: 27 April 2017

Accepted Date: 7 May 2017

Please cite this article as: Snellman, A., Rokka, J., Lopez-Picon, F.R., Helin, S., Re, F., Löyttyniemi, E., Pihlaja, R., Forloni, G., Salmona, M., Masserini, M., Solin, O., Rinne, J.O., Haaparanta-Solin, M., Applicability of [^{11}C]PIB micro-PET imaging for *in vivo* follow-up of anti-amyloid treatment effects in APP23 mouse model, *Neurobiology of Aging* (2017), doi: 10.1016/j.neurobiolaging.2017.05.008.

This is a PDF file of an unedited manuscript that has been accepted for publication. As a service to our customers we are providing this early version of the manuscript. The manuscript will undergo copyediting, typesetting, and review of the resulting proof before it is published in its final form. Please note that during the production process errors may be discovered which could affect the content, and all legal disclaimers that apply to the journal pertain.





ACCEPTED MANUSCRIPT

Applicability of [¹¹C]PIB micro-PET imaging for *in vivo* follow-up of anti-amyloid treatment effects in APP23 mouse model

Anniina Snellman^{a,b,c*}, Johanna Rokka^d, Francisco R. Lopez-Picon^{a,b}, Semi Helin^d, Francesca Re^e, Eliisa Löyttyniemi^f, Rea Pihlaja^{a,b}, Gianluigi Forloni^g, Mario Salmona^g, Massimo Masserini^e, Olof Solin^{d,h,i}, Juha O. Rinne^j, Merja Haaparanta-Solin^{a,b}

^aPET Preclinical Laboratory, Turku PET Centre, University of Turku, Tykistökatu 6 A, FI-20520 Turku, Finland

^bMedicity Research Laboratory, University of Turku, Tykistökatu 6 A, FI-20520 Turku, Finland

^cDrug Research Doctoral Programme, University of Turku, Turku, Finland

^dRadiopharmaceutical Chemistry Laboratory, Turku PET Centre, University of Turku, Kiinamylynkatu 4-8, FI-20520 Turku, Finland

^eDepartment of Health Sciences, University of Milano-Bicocca, Monza (MB), Italy

^fDepartment of Biostatistics, Turku University, Kiinamylynkatu 10, Medisiina C1, FI-20520 Turku, Finland

^gMario Negri Institute for Pharmacological Research, IRCCS-Istituto di Ricerche Farmacologiche "Mario Negri", Via Giuseppe la Masa 19, 20156 Milan, Italy

^hAccelerator Laboratory, Åbo Akademi University, Kiinamylynkatu 4-8, FI-20520, Finland

ⁱDepartment of Chemistry, University of Finland, Vatselankatu 2, FI-20014 Turun yliopisto, Turku, Finland

^jTurku PET Centre, Turku University Hospital, Kiinamylynkatu 4-8, FI-20520 Turku, Finland

*Corresponding author: Email address: aepakk@utu.fi (A.Snellman)

Abstract

In this study, we evaluated the anti-amyloid effect of functionalized nanoliposomes (mApoE-PA-LIP) in a mouse model of Alzheimer's disease (AD) with use of positron emission tomography (PET) and β -amyloid ($A\beta$) targeted tracer [^{11}C]PIB. APP23 mice were injected with mApoE-PA-LIP or saline (3 times per week for three weeks) and [^{11}C]PIB imaging was performed at baseline, after the treatment and after three months follow-up period, accompanied by $A\beta$ immunohistochemistry and ELISA. After the treatment, [^{11}C]PIB binding ratios between mApoE-PA-LIP and saline groups were equivalent in all analyzed brain regions; However, in the saline group, binding ratios increased from the baseline, whereas no increase was detected in the mApoE-PA-LIP group. During the additional follow-up, [^{11}C]PIB binding increased significantly from baseline in both groups, and binding ratios correlated with the immunohistochemically defined $A\beta$ load. This study further supports the use of [^{11}C]PIB PET imaging as a biomarker of $A\beta$ deposition in APP23 mice, and highlights the benefits of non-invasive follow-up, i.e. using baseline data for animal stratification and normalization of treatment effects to baseline values, for future anti-amyloid treatment studies.

Keywords: Alzheimer's disease; [^{11}C]PIB; PET; β -amyloid; liposomes; APP23

1. Introduction

Alzheimer's disease (AD) is a slowly progressing neurodegenerative disorder that at present affects approximately 36 million people worldwide. Unless significant improvements for prevention and treatment can be found, the number has been estimated to rise to 115 million by 2050 (Wimo, et al., 2014). The disease mechanism of AD is still not unraveled in detail; However, accumulation of beta-amyloid ($A\beta$) to extracellular plaques as well as the presence of soluble oligomeric forms ($A\beta_o$) have been suggested to be key events in the brain of AD patients, leading to other pathophysiological and neurotoxic changes, such as increased and spread tau pathology and synaptic dysfunction (Hardy and Selkoe, 2002, Karran and De Strooper, 2016). Since the postulation of the amyloid cascade hypothesis 25 years ago (Hardy and Higgins, 1992), there has been tremendous efforts to develop $A\beta$ targeted compounds, aiming to either prevent excess formation of $A\beta$ in the brain, or to remove already existing $A\beta$ deposits, for disease modifying treatment of AD (Karran and Hardy, 2014). Unfortunately, such compound has still not reached the market.

Non-invasive molecular imaging technique positron emission tomography (PET) is highly beneficial for research and drug discovery of CNS diseases, enabling the *in vivo* monitoring of various pathological processes, target engagement and treatment effects in human brain. For AD research, a positive amyloid PET scan obtained with $A\beta$ binding radiotracers such as [^{11}C]Pittsburgh Compound B ([^{11}C]PIB) is currently recognized as a valid biomarker of brain $A\beta$ deposition (Dubois, et al., 2014), and can be exploited in clinical $A\beta$ -centric drug trials as an inclusion criterion for AD patients in addition to longitudinal monitoring of $A\beta$ accumulation as a secondary outcome. Micro-PET imaging of $A\beta$ pathology in transgenic (Tg) mouse models of the disease using [^{11}C]PIB and other $A\beta$ -tracers provides an ideal translational *in vivo* method for preclinical proof-of-concept studies (Zimmer, et al., 2014), and to date, changes in $A\beta$ deposition have already been successfully followed *in vivo* using multiple mouse models of AD and different amyloid tracers (Brendel, et al., 2014, Maeda, et al., 2007, Manook, et al., 2012, Rominger, et al.,

2013,Snellman, et al., 2013,Snellman, et al., 2012,Zimmer, et al., 2014). However, even though the potential advantages of longitudinal *in vivo* amyloid PET for preclinical drug development have been suggested by the authors, micro-PET imaging of A β has still mainly contributed to the characterization of novel PET radiotracers and animal models rather than A β -targeted drugs.

Nanotechnology and different functionalized nanomaterials offer a novel innovative approach for therapy of CNS diseases, often made challenging by limited penetration of drugs to the brain through the blood–brain barrier (BBB) (Re, et al., 2012). Liposomes (LIPs) have been traditionally used as drug-carriers (Bozzuto and Molinari, 2015), however, functionalized LIPs have recently been developed also as potential AD therapeutics (Balducci, et al., 2014,Bana, et al., 2014,Mancini, et al., 2016,Re, et al., 2011). These LIPs are functionalized with two ligands, phosphatidic acid (PA) to bind A β (Gobbi, et al., 2010) and a modified peptide from the receptor-binding domain of apolipoprotein E containing amino acid residues 141–150 (mApoE) to increase BBB passage via the LDL receptor-mediated system (Re, et al., 2010). These LIPs, known as mApoE-PA-LIPs, have been seen to bind to A β_{1-42} *in vitro*, inhibit its aggregation, promote the rupture of already existing deposits, and enhance the efflux of A β_o in a BBB-model (Bana, et al., 2014,Mancini, et al., 2016). In subsequent *in vivo* studies, mApoE-PA-LIPs also decreased the amount A β_{1-42} , A β_o and A β deposits in the brain of APP-PS1 mice and significantly restored long-term recognition memory compared to a control group (Balducci, et al., 2014). These observed *in vivo* effects have been suggested to be exerted partially by an enhancement of spontaneous A β efflux from the brain via a peripheral sink effect (Mancini, et al., 2016).

The objective of this study was to validate the use of *in vivo* [^{11}C]PIB micro-PET imaging for following anti-A β treatment effects in preclinical studies by longitudinally evaluating the acute and long term effect of mApoE-PA-LIPs for cerebral A β deposition in the APP23 mouse model of AD.

2. Materials and Methods

2.1. Preparation and characterization of mApoE-PA-LIPs

Nanoliposomes known as mApoE-PA-LIPs were generated and characterized as described earlier (Balducci, et al., 2014) and were prepared freshly for each week of the study ($n = 3$). Cholesterol and sphingomyelin were obtained from Sigma-Aldrich (St. Louis, MO, USA), PA and Mal-PEG-PE from Avanti Polar Lipids, Ltd (Alabaster, AL, USA). The size of the LIPs was determined by dynamic light scattering before the mApoE functionalization and it was 190 ± 18 nm with a polydispersity index < 0.35 . The lipid concentration of mApoE-PA-LIPs was 15.6 ± 0.5 mM based on sphingomyelin content. LIP functionalization with mApoE peptide residue was carried out as described by Re and co-workers (Re, et al., 2010).

2.2. [^{11}C]PIB synthesis

[^{11}C]PIB was synthesized from cyclotron-produced [^{11}C]methane that was halogenated by gas phase reaction into [^{11}C]methyl iodide (Larsen, et al., 1997) and converted online into [^{11}C]methyl triflate (Jewett, 1992). After introducing the [^{11}C]methyl triflate into a solution of desmethyl precursor 6-OH-BTA-0 (0.6–1.0 mg) in acetone (200 μl) at 0 $^{\circ}\text{C}$, followed by 3 min reaction at 80 $^{\circ}\text{C}$, the product was purified in a HPLC column (YMC-Pack ODS-A, 5 μm , 10 \times 250 mm, YMC Co.,Ltd., Japan) and a solid phase extraction C18 cartridge (Sep-Pak[®] Light, Waters Corp., Milford, MA, USA). Ascorbic acid solution (Ascorell[®], 100 mg/ml, Sanorell Pharma GmbH, Germany) was used against radiolysis, that otherwise occurred during purification at specific activity (SA) levels over 1 TBq/ μmol . For the HPLC mobile phase, Ascorell[®] (2 ml) was added into 1 l of methanol/water (65:35 v/v). Solid phase extraction bulk dilution and washing solutions consisted of water (30 ml) and Ascorell[®] (50 μl). The product was extracted from the cartridge by ethanol, diluted with propylene glycol/0.1 M phosphate buffer mixture (1.5:8.5, v/v) to a $< 10\%$ ethanol level and filtered through a sterile filter (Millex GV, 0.22 μm , 33 mm, Merck Millipore Ltd.,

Ireland). An analytical HPLC column (Kinetex XB-C18, 2.6 μm , 3.00 \times 50 mm, Phenomenex Inc., USA), acetonitrile in H_3PO_4 (0.05 M, 25:75 v/v) mobile phase, 1 ml/min flow rate, 3.5 min run time and detectors in series for UV absorption (345 nm) and radioactivity were used for determination of identity, radiochemical purity and mass concentration. The SA of [^{11}C]PIB was 1280 ± 290 GBq/ μmol (21 batches) at the end of synthesis. The radiochemical purity exceeded 99% in all syntheses.

2.3. Animals

Male (n = 10) and female (n = 2) APP23 Tg mice, aged 16–17 months were obtained from Novartis (Basel, Switzerland). The APP23 mouse model expresses human APP751 with the Swedish double point mutation (K670M/N671L) driven by the neuron-specific mouse Thy-1.2 gene fragment as a promoter. A β immunoreactive plaques develop progressively starting from the frontal cortex (FC) and extending to the whole neocortex (NC) and hippocampus (HC) (Sturchler-Pierrat, et al., 1997). Mice were housed in individually ventilated cages, at an ambient temperature of 21 ± 3 °C and humidity of $55 \pm 15\%$. Lighting and dark-cycles altered in 12 hr shifts starting at 6:00 a.m. Mice had *ad libitum* access to soya-free chow (SDS RM3 (E) soya-free, 801710; Special Diets Service) and tap water. Animals were sacrificed after the last PET scan by cardiac puncture in Isoflurane anesthesia. The animal study was approved by the National Animal Experiment Board of Finland.

2.4. Experimental design

Figure 1 illustrates schematically the chronology of [^{11}C]PIB imaging and mApoE-PA-LIP treatment of APP23 mice. Mice were divided into two groups receiving either mApoE-PA-LIP (n = 5) or physiological saline (n = 7) as control. The separation of animals into two groups is described in Table 1. Animals were allocated into saline and mApoE-PA-LIP groups to preserve the same mean age in each. As illustrated in Figure 1, after initial [^{11}C]PIB scanning, mice received 100 μL intraperitoneal injections of either mApoE-PA-LIPs or physiological saline following the protocol

described earlier (Balducci, et al., 2014). APP23 mice over 15 months of age were used because they are known to have A β plaque formation already detectable by [^{11}C]PIB PET imaging (Snellman, et al., 2013). The pre-defined brain areas of interest were the FC, NC and HC, based on the abundance of A β deposition in the APP23 model (Snellman, et al., 2013, Sturchler-Pierrat, et al., 1997).

2.5. *In vivo* [^{11}C]PIB PET imaging

As illustrated in Figure 1, APP23 mice were repeatedly imaged with [^{11}C]PIB and an Inveon Multimodality PET/CT camera (Siemens Medical Solutions, Knoxville, TN, USA). The mice were anesthetized with 2.5% Isoflurane, and after a transmission scan for attenuation correction, [^{11}C]PIB was injected intravenously (10.3 ± 0.5 MBq, injected mass 3.4 ± 0.6 ng, SA 1085 ± 184 GBq/ μmol at the time of injection). PET data were collected for a 60 min period and divided into 51 time frames (30×10 s; 15×60 s; 4×300 s; 2×600 s) and reconstructed with use of 3D-OSEM. The voxel size was $0.8 \times 0.8 \times 0.79$ mm³. Dynamic images were co-registered with CT scans from the same mouse and a mouse brain template, and analyzed using Inveon Research Workplace 3.0 (Siemens Medical Solutions). Volumes of interest (VOIs) for the FC (15 mm³), NC (64 mm³), HC (12 mm³) and cerebellum (CB, 21 mm³), were defined by the used mouse brain template (Mouse MRI brain template, 2005).

2.6. *Analysis of PET data*

All data sets were analyzed without prior knowledge of the treatment status of the mice. The CB was used as the reference region because A β deposition does not occur in this region in APP23 mice (Sturchler-Pierrat and Staufenbiel, 2000). Regional time–activity curves were calculated for each VOI, and [^{11}C]PIB binding was quantified as bound-to-free binding ratios for the late washout phase (40–60 min p.i.) as previously described (Snellman, et al., 2013). Changes in binding ratios were calculated for follow-up intervals, as defined in Figure 1.

2.7. Tissue collection

As indicated in Fig. 1, after the last PET scan the brains from mApoE-PA-LIP (n = 4) and saline treated mice (n = 2) were dissected and the hemispheres were separated. The left hemisphere was frozen in chilled isopentane on dry ice, stored air-tight at -70°C and later cut into serial sagittal cryosections used for IHC. The right hemisphere was divided into the forebrain (without the olfactory system and brain stem) and CB, frozen in liquid nitrogen, and stored at -70°C for later preparation of brain homogenates for ELISA.

2.8 ELISA analysis

The right forebrain of each animal was homogenized in PBS, pH 7.4, containing protease inhibitors (Complete, Roche, Mannheim, Germany) and subjected to ultracentrifugation for 3 h ($100,000\times g$). The supernatant was collected and stored at -70°C prior to analysis as the PBS-soluble A β fraction. The pellet was further homogenized in 5 M Guanidine HCl buffered to pH 8.0 with 0.05 M Tris-HCl with protease inhibitors, agitated for 3 h and stored at -70°C prior to analysis as the PBS-insoluble/Guanidine HCl-soluble A β -fraction. Finally, the amount of A β_{1-40} and A β_{1-42} from each sample was quantified according to the protocol given for the used ELISA assay kit (Human A β_{1-40} and A β_{1-42} ELISA, Thermo Fisher Scientific, Waltham, MA, USA). The results were normalized on the basis of the wet brain tissue weight and expressed as nmol/mg brain tissue (PBS-insoluble A β) or pmol/mg brain tissue (PBS-soluble A β).

2.9. Thioflavin S staining and immunohistochemistry

The left hemisphere of each mouse was sliced longitudinally into 14 μm cryosections using CM3050S cryostat (Leica Biosystems, Nussloch, Germany). After each of four sections was placed on a different slide, a slice of approximately 0.5 mm thickness was removed and discarded. Four more 14 μm sections were then sliced and each placed sequentially on one of the four slides. This treatment of mouse brains continued until a total of six sections were mounted per slide. Each slide,

thus, contained six sections so that the sections with respect to their locations in the brain were separated from each other by 0.5 mm. Slides with adjacent sections were treated separately as follows.

For Nissl staining, fresh-frozen sections were post-fixed in 4% paraformaldehyde for 30 min, rinsed with PBS, and incubated in cresyl violet solution (Sigma-Aldrich Co., St. Louis, MO, USA), for 20 min. Sections were imaged with a 3DHistech Slide Scanner and evaluated using CaseViewer software v. 1.3 (3DHistech Ltd., Budapest, Hungary).

ThS (Sigma-Aldrich, St. Louis, MO, USA) staining was carried out as described (Snellman, et al., 2012) and evaluated with a SteREO Lumar V12 microscope. Images were captured with an Axiocam HRm camera (Zeiss, Jena, Germany). For quantification of A β load, microscope images with 10 \times (FC, NC) and 4 \times (HC) magnification were captured with use of an Olympus BX60 microscope and an Olympus DP71 camera (Olympus, Tokyo, Japan).

Fresh-frozen sections used for anti-A β_{1-40} (Millipore, Temecula, CA, USA), anti-A β_{1-42} (Millipore, Temecula, CA, USA) and anti-Iba-1 (Wako Pure Chemical Industries, Ltd., Osaka, Japan) IHC were first fixed in 4% paraformaldehyde for 30 min. For anti-A $\beta_{1-40/1-42}$ staining sections were also pre-treated with > 95% formic acid for 10 min. Sections were then incubated in a blocking solution (0.3% Triton X-100 in PBS (pH 7.4), 2% BSA, 2% normal goat serum) for 30 min for anti-A $\beta_{1-40/1-42}$ staining or 2 h for anti-Iba-1 staining, and subsequently with primary antibodies at 8 °C for 48 h for A $\beta_{1-40/1-42}$ staining (dilution of 1:400) or 24 h for Iba-1 staining (dilution of 1:1000). After washing, the sections were incubated with a biotin-conjugated goat anti-rabbit secondary antibody (Invitrogen, Camarillo, CA, USA, dilution 1:500) for 60 min, and with avidin–peroxidase conjugate (Vectastain ABC Kit, Vector Laboratories, Burlingame, CA, USA) for 30 min, before visualizing the staining using 3,3-diaminobenzidine tetrahydrochloride (Sigmafast, Sigma-Aldrich Co., St. Louis, MO, USA). For Nissl counter stain, the Iba-1 stained sections were subsequently incubated

in cresyl violet solution for 10 min before dehydration and mounting. Sections were imaged with a 3DHitech Slide Scanner and evaluated using CaseViewer software v. 1.3.

2.10. Quantification of A β deposition

To estimate the area of ThS, A β_{1-40} , and A β_{1-42} stained A β plaques, serial microscope images from stained sections (0.5 mm intervals) of each APP23-mouse were obtained from different locations. 10 \times magnification was used in the FC (total 12 images per stain, from four sections) and NC (total 42 images per stain, from six sections), and 4 \times magnification for the HC (total six images per stain from, six sections). Images were transformed to 8-bit black-and-white images and the percentage of stained A β positive area from the total area was calculated using Image J 1.43u (Wayne Rasband, National Institutes of Health, MD, USA). The average percentages were calculated for each brain region.

2.11. Data analysis and statistics

Data are given as mean \pm standard deviation (SD) or individual values if $n < 3$. The following calculations were carried out with use of GraphPad Prism software v. 5.01 (GraphPad Software, San Diego, CA, USA). Differences in injected doses, injected mass, SA, age and baseline binding ratios between mApoE-PA-LIP and saline groups were tested with unpaired t-test, and correlations between IHC and [^{11}C]PIB binding ratios with Pearson's correlation. Differences in changes in binding ratios over time between mApoE-PA-LIP and saline groups and differences in binding ratios over time within groups were tested using hierarchical linear mixed models where repeated measuring time points were handled as within factor and groups as between factor. This repeated measures analysis was performed with SAS $^{\text{®}}$, v. 9.4 for Windows (SAS Institute Inc., Cary, NC, USA). Differences were considered statistically significant if $p < 0.05$ (two-tailed).

3. Results

3.1. Animals and study deviations

During the longitudinal imaging study, three APP23 mice died before study termination: two male mice from the saline group during the treatment period and one male mouse from the mApoE-PA-LIP group during the follow-up period. These dropout animals did not show signs of illness or any abnormality at the time of imaging and thus the obtained data from these mice was included in the final analysis. The data points obtained from the dropout animals, and their effect on the obtained group means are clearly indicated in Fig. S1. Brains from three saline treated mice (two females, one male) could not be used for histological or biochemical analysis due to technical difficulties.

3.2 Longitudinal *in vivo* [¹¹C]PIB imaging

The baseline and follow-up [¹¹C]PIB binding ratios for mApoE-PA-LIP and saline groups are presented at Table 2, while PET images of representative mApoE-PA-LIP and saline treated APP23 mice and quantified [¹¹C]PIB binding ratios for each mouse are illustrated in Figure 2. Prior to treatment of mice as shown in Fig. 2A (0 months), cortical [¹¹C]PIB binding was already visible in the summed (40–60 min p.i.) PET images of most mApoE-PA-LIP and saline injected mice. Nonetheless, binding ratios at baseline varied from -0.11 to 0.59, indicating a large variation in cerebral A β load among the age-matched APP23 mice prior to initiation of treatment. Mean binding ratios at baseline were higher in mApoE-PA-LIP group in all analyzed brain regions, and the difference reached statistical significance in the HC ($p = 0.02$, unpaired t-test).

After the three week period of treatment, as summarized in Table 2, the binding ratios remained close to baseline levels in mApoE-PA-LIP group (mean change -0.002 ± 0.31 , 0.07 ± 0.20 and -0.01 ± 0.17 for FC, NC and HC, respectively), while increases were detected in the saline group (mean increase 0.19 ± 0.20 , 0.10 ± 0.08 and 0.13 ± 0.10 for FC, NC and HC, respectively). However, due to large variations within both groups, the differences between the groups were not statistically

significant for any of the brain regions ($p = 0.21$ (FC), $p = 0.61$ (NC) and $p = 0.14$ (HC), hierarchical linear mixed model).

Three months after termination of the mApoE-PA-LIP treatment, as seen in Table 2 [^{11}C]PIB binding had increased significantly from baseline in both mApoE-PA-LIP and saline groups in all analyzed brain regions. However, differences in the changes in the binding ratios between the two groups were not significant over the entire time period, as confirmed by the calculated p -values for the FC ($p = 0.35$), NC ($p = 0.86$), and HC ($p = 0.21$). Changes in the binding ratios for the entire time period are illustrated in Figs. 2B–D for the FC, NC and HC brain areas, respectively.

3.3. $A\beta_{1-40}$ peptide levels in the brain

Results from APP23 mouse brain homogenate analysis by ELISA showed similar brain $A\beta_{1-40}$ and $A\beta_{1-42}$ levels in mApoE-PA-LIP and saline treated APP23 mice at follow-up 2. Total PBS-insoluble $A\beta_{1-40}$ and $A\beta_{1-42}$ concentrations were 27.6 ± 6.0 and 5.6 ± 0.4 nmol/g in the mApoE-PA-LIP group ($n = 4$) and $26.4/23.5$ and $4.8/5.4$ nmol/g in saline-treated mice ($n = 2$). The concentrations of PBS-soluble $A\beta_{1-40}$ and $A\beta_{1-42}$ were much lower, 2.3 ± 1.0 and 0.4 ± 0.3 pmol/g in the mApoE-PA-LIP group and $2.4/2.0$ and $0.2/0.3$ pmol/g in the saline group.

3.4. $A\beta$ deposition in the brain

All amyloid stainings revealed abundant $A\beta$ deposition in the brain of both mApoE-PA-LIP and saline treated APP23 mice at follow-up 2. Large and ubiquitous ThS-fluorescent (Fig. 3) and anti- $A\beta_{1-40}$ -immunoreactive (Fig. 4) $A\beta$ deposits were observed around the NC and HC in both groups. Anti- $A\beta_{1-42}$ immunoreactive deposits (Fig. 5) were smaller and less abundant than anti- $A\beta_{1-40}$ or ThS stained deposits, as expected in the used APP23 model that mainly expresses compact, fibrillary plaques and $A\beta_{1-40}$ over $A\beta_{1-42}$ (Sturchler-Pierrat and Staufenbiel, 2000). The reference region (CB) was free of $A\beta$ deposition in all mice at all times. Quantified ThS, anti- $A\beta_{1-40}$ and anti- $A\beta_{1-42}$ stained $A\beta$ -plaque load percentages for mApoE-PA-LIP and saline groups are

presented in Table 2. The plaque load was equivalent in mApoE-PA-LIP and saline injected mice in all analyzed brain areas.

Significant positive correlation was found between the [^{11}C]PIB binding ratios and ThS (Pearson's $r = 0.71$, $p = 0.001$), anti-A β_{1-40} (Pearson's $r = 0.88$, $p < 0.0001$) and anti-A β_{1-42} -stained total A β plaque area (Pearson's $r = 0.59$, $p = 0.001$) when PET imaging data and histological data from all analyzed brain areas were pooled (Fig. 6).

3.5. Microglial activation in the brain

Iba-1 immunostaining, a marker for microglial activation, revealed abundant microgliosis around the brain in both mApoE-PA-LIP and saline injected APP23-mice. Most intense staining was seen to surround the existing A β deposits. Staining intensities were not quantified further; however, representative microscope images from the cortex, HC and CB are presented in Fig. S1.

4. Discussion

Because of the increasing prevalence of AD, there is a strong need for both novel-disease modifying therapies, as well as improved methods that could benefit and speed up the drug development process. Here we report that treatment effects of nanoliposomes, known as mApoE-PA-LIPs, functionalized to bind and discard A β in the brain, were followed longitudinally in APP23 mouse model *in vivo* with use of micro-PET and amyloid PET tracer [^{11}C]PIB. We suggest that in addition to characterizing new PET tracers and animal models, micro-PET combined with mouse models of A β deposition would be a valuable tool for preclinical evaluation of novel anti-amyloid compounds for AD.

4.1. mApoE-PA-LIP treatment effects in APP23 mouse model of AD

The mApoE-PA-LIPs have previously been shown reduce A β pathology *in vivo* in APP/PS1 Tg mouse model (Balducci, et al., 2014). In that model, peripheral administration of mApoE-PA-LIP

led to decreased brain $A\beta_{1-40}$, $A\beta_{1-42}$ and $A\beta_o$ levels, reduction in the number of $A\beta$ plaques, and increase in plasma $A\beta$ levels (Balducci, et al., 2014, Mancini, et al., 2016). However, due to the low [^{11}C]PIB binding that has been previously reported in old APP/PS1 mice even with abundant histologically confirmed $A\beta$ deposition (Snellman, et al., 2013), this model could not be used for further [^{11}C]PIB PET imaging experiments and the APP23 model was exploited instead.

A pilot study, where [^{11}C]PIB PET was used to evaluate mApoE-PA-LIP effects in three APP23 Tg mice was included in the previously published study by Balducci and co-workers (Balducci, et al., 2014). In that study, mApoE-PA-LIP-treated APP23 mice showed very low [^{11}C]PIB binding ratios similar to wild type mice at baseline (15 months), and interestingly also at both follow-ups, raising interest to further *in vivo* investigation of possible long term effects of mApoE-PA-LIP treatment. Based on these results, we designed our study to include more animals, a proper control group receiving saline injections and similar additional follow-up period of three months after the termination of mApoE-PA-LIP administration. However, the [^{11}C]PIB PET imaging data presented here differs from the previously published results; In our study we saw a trend of slower increase in [^{11}C]PIB binding from baseline immediately after the treatment period in mApoE-PA-LIP group in comparison to saline group, suggesting inhibition of plaque formation during the treatment period. However, during the additional follow-up, [^{11}C]PIB retention increased significantly from baseline in both groups and equivalent immunohistochemically verified $A\beta$ load was detected at study termination after follow-up 2. Thus, no long term differences between groups were detected.

In our study, the APP23 Tg mice were slightly older (16–17 months) at the initiation of the study and had higher quantified baseline [^{11}C]PIB binding ratios, suggesting more abundant $A\beta$ deposition in the brain at the time when mApoE-PA-LIP treatment was initiated. The data from these studies could suggest, that earlier (preventional) initiation of mApoE-PA-LIP treatment in APP23 Tg mice, at a time when $A\beta$ deposition is still below the detection level of [^{11}C]PIB, would lead to more efficient inhibition of $A\beta$ aggregation, possibly by mApoE-PA-LIPs binding to the

soluble A β forms, and further enhancing their efflux from the brain via the peripheral sink effect reported by Mancini and co-workers (Mancini, et al., 2016). For therapeutic studies, initiated at a time when abundant A β deposition and increased [^{11}C]PIB retention in the FC is already present, longer or continuous treatment schedules would most probably be needed to obtain similar long-term effect. This view is supported by the abundant large and dense cored A β deposits in older APP23 Tg mice and the constantly increasing A β levels and plaque formation in this model still at the investigated age (16–20 months). However, the unfortunate small sample size in the *in vitro* experiments at follow-up 2, especially in the saline group, should be kept in mind when interpreting the results further.

4.2. Applicability of small animal [^{11}C]PIB PET for preclinical anti-amyloid drug development

Even though the first attempts to use [^{11}C]PIB PET imaging for detecting cerebral A β deposition in Tg mouse models resulted in contradictory results (Klunk, et al., 2005, Maeda, et al., 2007), more recent studies have already demonstrated the usability of this method for non-invasive monitoring of histologically confirmed cerebral amyloidosis in various Tg mouse models, such as the APP23 mice (Maeda, et al., 2007, Snellman, et al., 2013), APP/PS1 ARTE-10 mice (Manook, et al., 2012) and APP/PS1-21 mice (Maier, et al., 2014). However, even after several studies confirming the usability of [^{11}C]PIB and other ^{18}F -labeled amyloid imaging PET tracers for preclinical imaging (Brendel, et al., 2015a, Rominger, et al., 2013, Snellman, et al., 2014, Sérière, et al., 2015), to our knowledge, only one longitudinal study where a potential disease-modifying drug for AD was evaluated has been published to date (Brendel, et al., 2015b). In this study, Brendel and colleagues showed that *de novo* plaque formation in APP-Swe mice was inhibited during treatment with a novel gamma-secretase modulator RO5506284, and the effect could be predicted by longitudinal *in vivo* [^{18}F]florbetaben micro-PET imaging (Brendel, et al., 2015b). In our study, mApoE-PA-LIP treatment resulted in unchanged [^{11}C]PIB binding during the treatment in mApoE-PA-LIP group, in comparison to clear increase in the saline group, even though statistical significance could not be

reached. However, high variability in [^{11}C]PIB binding ratios at baseline was detected in APP23 mice at this age, and consequently the group level differences in binding ratios over time did not reach statistical significance in any of the analyzed brain areas. Similar high variation in radiotracer binding at baseline that was seen in our study was also reported by Brendel and co-workers for the APP-swe model (Brendel, et al., 2015b). The results from both of these studies clearly highlight the advantage of micro-PET and non-invasive longitudinal follow-up of anti-amyloid treatment effects in comparison to cross-sectional comparison of treatment and control groups: By longitudinal follow-up of PET tracer uptake in each animal it is possible to minimize the bias caused by high variation in A β levels even in age-matched Tg mice that have been reported for most mouse models of A β deposition. In addition, the method enables animal stratification based on their baseline binding ratios and estimated levels of A β pathology. For future studies this approach is highly recommended.

4.3 Study limitations

The lack of histological data verifying the level of A β deposition immediately after the mApoE-PA-LIP treatment period can be considered as a limitation of our study. However, after the final PET scan, A β load in the brain of Tg mice was quantified with ThS and IHC, and a positive correlation with the quantitated PET binding ratios was observed, further supporting the validity of brain [^{11}C]PIB retention as a biomarker for A β deposition in this Tg mouse model. Rather than a weakness, this could be seen as the benefit of *in vivo* PET methodology, where fewer animals are needed for producing high quality data with repeated *in vivo* measurements. In addition, as discussed before, longitudinal study design enables analyzing relative changes from baseline values, rather than sole differences between interventional and control groups after treatment, that most likely are affected by the considerable variation in the amount of A β deposition that has been reported for APP23 mice and most other Tg models (Sturchler-Pierrat, et al., 1997).

The binding of mApoE-PA-LIPs to different forms of A β *in vitro* have been previously investigated by using A β_{1-42} and its aggregates (Bana, et al., 2014, Gobbi, et al., 2010, Mancini, et al., 2016), and thus the rationale of using the APP23 mouse model expressing more A β_{1-40} than A β_{1-42} for this study could be questioned. However, in the *in vivo* study by Balducci and colleagues, the mApoE-PA-LIP treatment was seen to decrease also soluble and insoluble A β_{1-40} levels in the brain of APP/PS1 mice, suggesting that mApoE-PA-LIP binding is not restricted to A β_{1-42} (Balducci, et al., 2014). In addition, situation in human AD is similar to the APP23 model, as A β_{1-42} comprises only 10% of the total A β levels (Hempel, et al., 2010). Due to these reasons the usage of the APP23 model in our opinion is justified and future experiments with preventative study design and longer mApoE-PA-LIP treatment period including also another PET scan in the middle of the treatment would give more information about the A β clearing effects of mApoE-PA-LIPs in this model.

4.4 Recommendations for future studies

The study design presented here includes also parts that could be improved and should be carefully considered when planning future interventional small animal imaging studies. First, even though it was known that the used repeated measures analyses is more powerful than one time-point approach (unpaired t-test), the animal number in this study was still relatively low, and could be the reason for the difficulties in detecting significant treatment effects between the groups. To avoid this, sample size calculations should be performed also for preclinical studies to increase their translational value. If we would use the data from this study and plan a future study based on how the mApoE-PA-LIP treated mice behaved in the pilot study (Balducci, et al., 2014), the mean baseline binding ratio of 0.4 could be estimated to remain unchanged at follow-up 2 in mApoE-PA-LIP group (SD was at greatest 0.25 for mApoE-PA-LIP group) and rise to 0.9 in the saline group (SD was at greatest 0.33). If we then calculate the sample size with 80% power and 0.05 significance level (two-tailed), we end up with 7 mice per group. According to this information, our study was approaching the optimal sample size. However, as previously discussed, the mApoE-PA-

LIP group did not behave as we expected based on the pilot study, as significant increases in the binding ratios were detected at follow-up 2. In addition, more animals should always be added to cover the possible dropouts during the study period that can be expected when aged AD models are used.

Second, animals with mixed gender were included, and both females were allocated to the saline group. Because the level of A β pathology has previously been reported to vary between male and female APP23 mice (Sturchler-Pierrat and Staufenbiel, 2000), it would be ideal to include only males or females for intervention studies. However, in this study, the baseline binding ratios of the two female mice were seen to fit inside the observed variation in the male mice, and because repeated measurements were performed, the females were included to increase the relatively small sample size. Nevertheless, for future studies mixing genders is not recommended.

Third, also the observed variation in the baseline binding ratios between age-matched groups was an unwanted finding in our study. For future studies, allocation of animals into groups based on their baseline binding ratios is highly recommended as an alternative to solely age-matching the groups. With this approach the groups could be better balanced and the accidental assignment of animals with very high or very low level of A β -pathology in one group could be avoided.

5. Conclusion

Shown here, the [^{11}C]PIB binding in APP23 mouse brain correlates well with the existing A β pathology and can thus be used as a biomarker to evaluate longitudinal changes in cerebral A β deposition *in vivo*. The data from this study further supports the use of longitudinal *in vivo* micro-PET follow-up of individual APP23 Tg mice in the preclinical phase of AD drug development to increase the quality of the data and translation of the results to clinical settings.

ABBREVIATIONS

[¹¹ C]PIB	[¹¹ C]Pittsburgh compound B
AD	Alzheimer's disease
APP	Amyloid precursor protein
A β	Beta-amyloid
CB	Cerebellum
CNS	Central nervous system
CT	Computed tomography
ELISA	Enzyme-linked immunosorbent assay
FC	Frontal cortex
HC	Hippocampus
Iba-1	Ionized calcium-binding molecule 1
LIPs	Liposomes
LDL	Low density lipoprotein
mApoE	Modified peptide derived from the receptor binding domain of apolipoprotein E
NC	Neocortex
OSEM	Ordered-Subsets Expectation Maximization
p.i.	post injection
PA	Phosphatidic acid
PBS	Phosphate buffered saline
PET	Positron emission tomography
Tg	Transgenic
ThS	Thioflavin S
VOI	Volume of interest

Acknowledgements

We thank the staff of the Accelerator Laboratory, Radiopharmaceutical Chemistry Laboratory and MediCity Research Laboratory for all assistance. Martti Kaasalainen and Jarno Salonen are acknowledged for assistance in particle characterization. Professor Marvin Mäkinen is acknowledged for valuable discussions and comments on the manuscript. The APP23 mice were used with the kind permission of Mathias Staufenbiel and Novartis.

This work was supported by the European Community's Seventh framework Programme (FP7/2007-2013) under grant agreements no. 212043; state funding for university level health research, Turku University Hospital (ERVA); the Finnish Cultural Foundation; the Maud Kuistila Memorial Foundation and Drug Research Doctoral Programme, University of Turku Graduate School.

Disclosure statement

The authors have no conflicts of interest to disclose.

Figure legends

Fig. 1. Chronology of [^{11}C]PIB imaging and mApoE-PA-LIP treatment of transgenic APP23 mice. The mice were imaged with [^{11}C]PIB before and after the three weeks treatment with mApoE-PA-LIP or physiological saline as control. After the final PET scan, animals were sacrificed, brains were dissected and A β load was analyzed from brain cryosections and brain tissue homogenates with use of immunohistochemistry (IHC) and Enzyme-linked immunosorbent assay (ELISA).

Fig. 2. Longitudinal changes in [^{11}C]PIB binding in mApoE-PA-LIP (red) and saline injected (blue) APP23 mice. (A) Summed (40–60 min p.i.) PET images of individual mApoE-PA-LIP and saline treated mice illustrate [^{11}C]PIB binding at baseline (age 16 months), at first follow-up immediately after the treatment (age 17 months) and at second follow-up three months after the treatment period (age 20 months). Quantified binding ratios as group means and changes in binding ratios between different time points are also presented for (B) frontal cortex, (C) neocortex and (D) hippocampus. The dotted line connects the data obtained from the two individual mice illustrated in Fig. 2A.

Fig. 3. ThS staining of fibrillar A β deposition in APP23 mice at follow-up 2. (A) Figure presents sagittal summed PET images (40–60 min p.i.), sagittal thioflavin S (ThS) stained brain sections and higher magnifications obtained from the neocortex (NC), hippocampus (HC) and cerebellum (CB) of representative mApoE-PA-LIP and saline injected mice at follow-up 2. In both groups [^{11}C]PIB binding and large fibrillar ThS-stained deposits were seen around the NC and in the HC. The cerebellum was free of fibrillar A β deposition. The age of the animals was 20–21 months. (B) From the stained sections ThS stained area as a percentage was calculated from the frontal cortex, NC and HC. A β accumulation in the brain was equivalent between groups. Scale bars, 200 μm (NC, CB); 500 μm (HC).

Fig. 4. Anti-A β_{1-40} stained A β deposition in APP23 mice at follow-up 2. (A) Figure presents sagittal brain sections with Nissl (cresyl violet) and anti-A β_{1-40} staining, and higher magnifications from the

neocortex (NC), hippocampus (HC) and cerebellum (CB) of representative mApoE-PA-LIP and saline treated mice at follow-up 2. Abundant anti-A β_{1-40} positive amyloid plaques were seen around the NC and in HC. The cerebellum was free of A β_{1-40} pathology. The age of the animals was 20–21 mo. (B) Anti-A β_{1-40} -positive area as a percentage was also calculated for the frontal cortex, NC and HC. No differences were seen in the anti-A β_{1-40} stained area in the brain between groups. Scale bars, 200 μm (NC, CB); 500 μm (HC).

Fig. 5. Anti-A β_{1-42} -positive A β deposition in APP23 mice at follow-up 2. (A) Figure presents sagittal brain sections with Nissl (cresyl violet) and anti-A β_{1-42} staining, and higher magnification from the neocortex (NC), hippocampus (HC) and cerebellum (CB) of representative mApoE-PA-LIP and saline treated mice 3 months after the treatment period. As expected, less intense staining and a lower amount of anti-A β_{1-42} positive deposits were seen in the NC and HC than with anti-A β_{1-40} . The cerebellum was free of A β_{1-42} pathology. The age of the animals was 20–21 mo. (B) Anti-A β_{1-42} positive area as a percentage was also calculated for the frontal cortex, NC and HC. No differences were seen in the anti-A β_{1-42} stained area in the brain between groups. Scale bars, 200 μm (NC, CB); 500 μm (HC).

Fig. 6. Correlation of *in vivo* [^{11}C]PIB binding ratios and A β deposition in APP23 mice. Pearson's correlations were calculated between quantitated PET [^{11}C]PIB binding ratios (B/F $_{40-60}$) and the amount of A β deposition in the frontal cortex (FC), neocortex (NC) and hippocampus (HC) of (A) thioflavin S, (B) anti-A β_{1-40} , and (C) anti-A β_{1-42} -stained brain sections of the same individual mice three months after the mApoE-PA-LIP or saline treatment period. Significant, positive correlations were detected between brain A β plaque load and *in vivo* [^{11}C]PIB binding ratios.

Tables and captions

Table 1. Summary of the two experimental groups. Data are given as mean \pm standard deviation (SD). Abbreviations: F, female; M, male; SA_{inj}, specific activity at the time of injection; Tg, transgenic.

		Treatment group	Control group	<i>p</i>-value
Strain		APP23 Tg	APP23 Tg	
Sex		M	M, F	
Treatment		mApoE-PA-LIP	Saline	
N	<i>scan 1</i>	5	7	
	<i>scan 2</i>	5	5	
	<i>scan 3</i>	4	5	
	<i>ex vivo</i>	4	2	
Age (mo)	<i>scan 1</i>	16.4 \pm 0.4	16.6 \pm 0.5	0.56
	<i>scan 2</i>	17.4 \pm 0.4	17.8 \pm 0.5	0.53
	<i>scan 3</i>	20.5 \pm 0.4	20.6 \pm 0.5	0.77
Weight (g)	<i>scan 1</i>	32 \pm 5	34 \pm 7	0.64
	<i>scan 2</i>	32 \pm 6	35 \pm 8	0.59
	<i>scan 3</i>	30 \pm 4	35 \pm 7	0.46
Premature deaths		1	2	
Injected dose (MBq)		10.4 \pm 0.5	10.3 \pm 0.6	0.86
Injected mass (ng)		5.9 \pm 1.6	6.5 \pm 2.5	0.50
SA_{inj} (GBq/μmol)		659 \pm 143	640 \pm 219	0.78

Table 2. Summary of the baseline and follow-up [^{11}C]PIB binding ratios and quantified beta-amyloid plaque ($\text{A}\beta$) load at follow-up 2 for mApoE-PA-LIP and saline groups. * $p < 0.05$, ** $p < 0.01$, *** $p < 0.001$, hierarchical linear mixed models, comparison to baseline [^{11}C]PIB binding ratios. # $p < 0.05$, unpaired t-test, comparison of baseline values between groups. Abbreviations: FC, frontal cortex; HC, hippocampus; NC, neocortex; ThS, Thioflavin S.

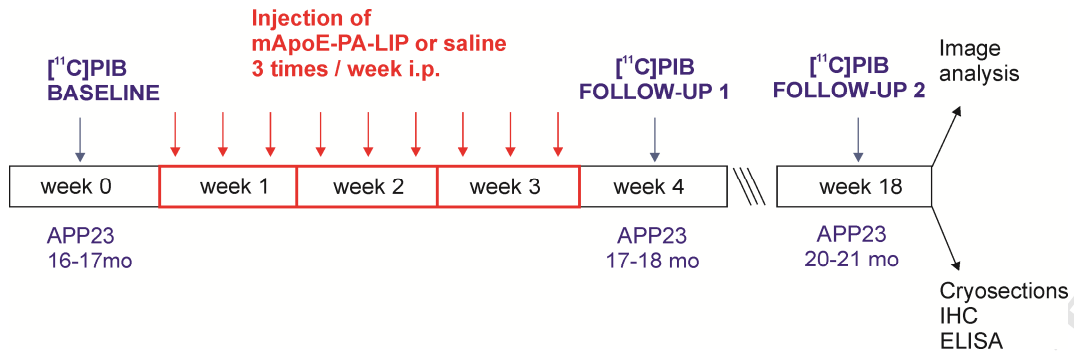
[^{11}C]PIB binding ratios	mApoE-PA-LIP (n = 4-5)			Saline (n = 5-7)		
	FC	NC	HC	FC	NC	HC
<i>Baseline</i>	0.41 ± 0.14	0.24 ± 0.07	0.17 ± 0.14#	0.21 ± 0.27	0.11 ± 0.19	0.02 ± 0.06#
<i>Follow-up 1</i>	0.41 ± 0.25	0.30 ± 0.18	0.17 ± 0.23	0.46 ± 0.28	0.25 ± 0.19	0.15 ± 0.08*
<i>Follow-up 2</i>	0.99 ± 0.21***	0.70 ± 0.24***	0.48 ± 0.21**	0.90 ± 0.33***	0.65 ± 0.29***	0.43 ± 0.10***
A β plaque load (%)	mApoE-PA-LIP (n = 4)			Saline (n = 2)		
<i>ThS</i>	5.2 ± 1.1	4.4 ± 0.3	1.4 ± 0.6	5.3/5.5	4.9/4.4	1.5/1.8
<i>Aβ_{40}</i>	5.2 ± 0.7	4.2 ± 0.7	1.7 ± 0.4	6.5/5.1	4.6/3.9	2.4/2.4
<i>Aβ_{42}</i>	3.0 ± 1.0	2.4 ± 0.6	1.3 ± 0.2	3.2/2.2	2.6/2.0	1.1/1.7

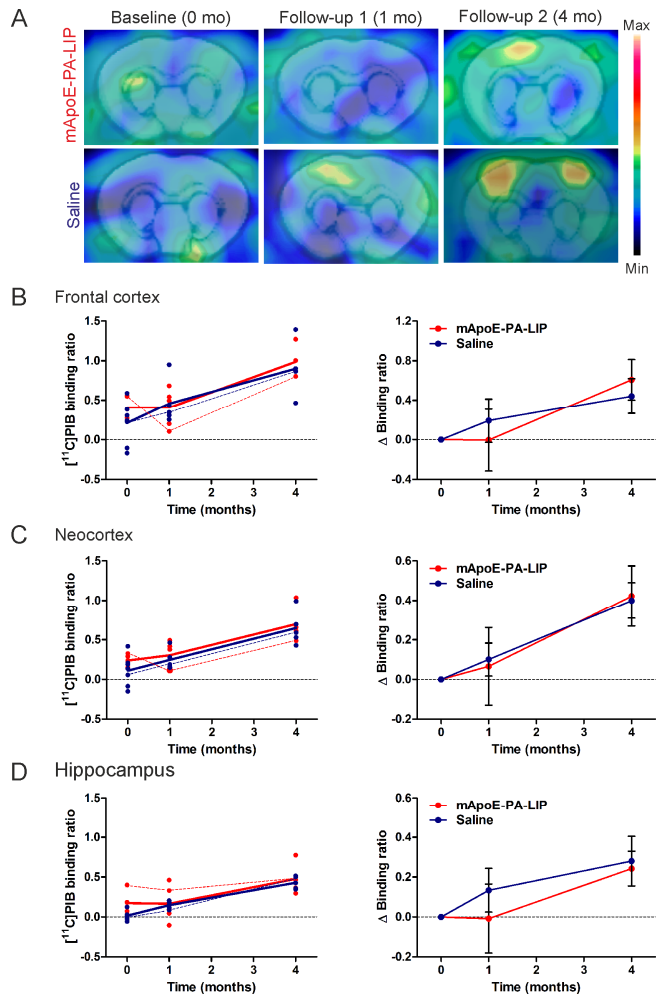
References

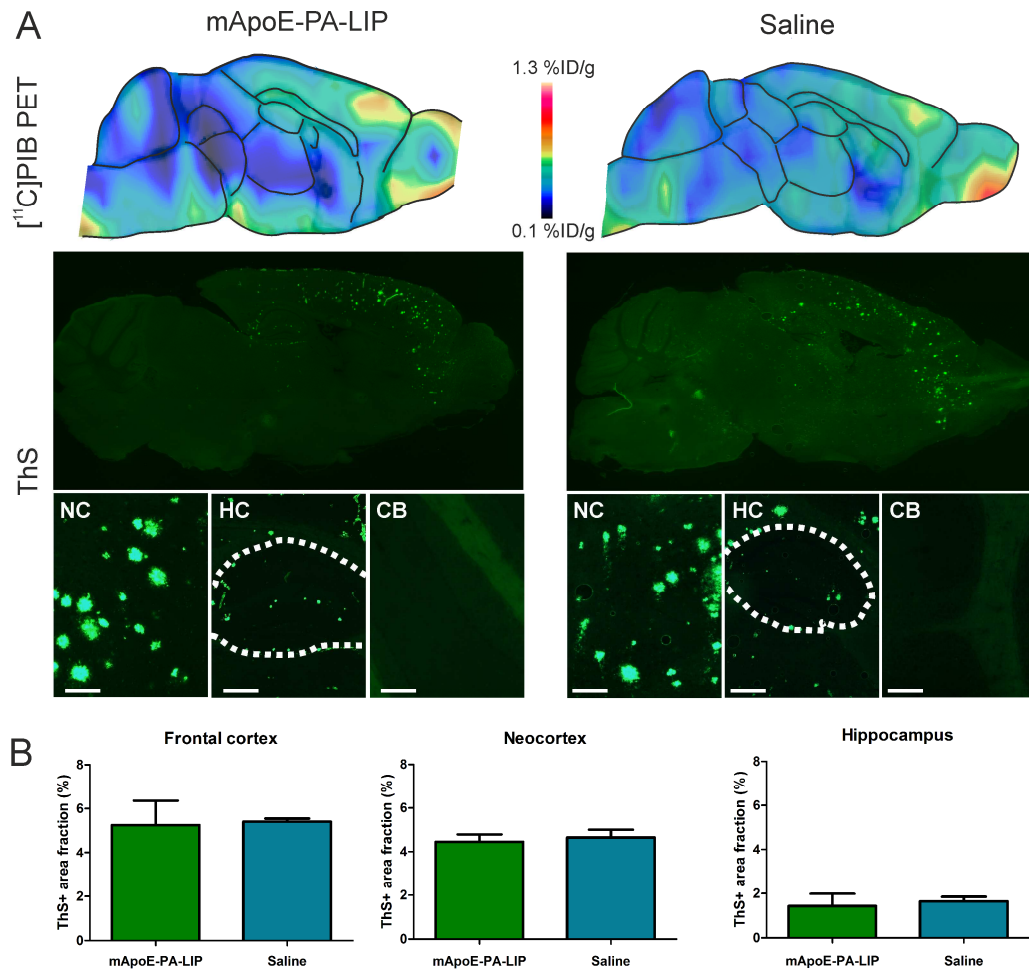
- Balducci, C., Mancini, S., Minniti, S., La Vitola, P., Zotti, M., Sancini, G., Mauri, M., Cagnotto, A., Colombo, L., Fiordaliso, F., Grigoli, E., Salmona, M., Snellman, A., Haaparanta-Solin, M., Forloni, G., Masserini, M., Re, F. 2014. Multifunctional liposomes reduce brain β -amyloid burden and ameliorate memory impairment in Alzheimer's disease mouse models. *J Neurosci* 34(42), 14022-31. doi:10.1523/JNEUROSCI.0284-14.2014.
- Bana, L., Minniti, S., Salvati, E., Sesana, S., Zambelli, V., Cagnotto, A., Orlando, A., Cazzaniga, E., Zwart, R., Scheper, W., Masserini, M., Re, F. 2014. Liposomes bi-functionalized with phosphatidic acid and an ApoE-derived peptide affect A β aggregation features and cross the blood-brain-barrier: implications for therapy of Alzheimer disease. *Nanomedicine* 10(7), 1583-90. doi:10.1016/j.nano.2013.12.001.
- Bozzuto, G., Molinari, A. 2015. Liposomes as nanomedical devices. *Int J Nanomedicine* 10, 975-99. doi:10.2147/IJN.S68861.
- Brendel, M., Delker, A., Rötzer, C., Böning, G., Carlsen, J., Cyran, C., Mille, E., Gildehaus, F.J., Cumming, P., Baumann, K., Steiner, H., Haass, C., Herms, J., Bartenstein, P., Rominger, A. 2014. Impact of partial volume effect correction on cerebral β -amyloid imaging in APP-Swe mice using [(18)F]-florbetaben PET. *Neuroimage* 84, 843-53. doi:10.1016/j.neuroimage.2013.09.017.
- Brendel, M., Jaworska, A., Griebinger, E., Rötzer, C., Burgold, S., Gildehaus, F.J., Carlsen, J., Cumming, P., Baumann, K., Haass, C., Steiner, H., Bartenstein, P., Herms, J., Rominger, A. 2015a. Cross-Sectional Comparison of Small Animal [18F]-Florbetaben Amyloid-PET between Transgenic AD Mouse Models. *PLoS One* 10(2), e0116678. doi:10.1371/journal.pone.0116678.
- Brendel, M., Jaworska, A., Herms, J., Trambauer, J., Rötzer, C., Gildehaus, F.J., Carlsen, J., Cumming, P., Bylund, J., Luebbers, T., Bartenstein, P., Steiner, H., Haass, C., Baumann, K., Rominger, A. 2015b. Monitoring of chronic γ -secretase modulator treatment by serial amyloid-PET. *Mol Psychiatry* 20(10), 1141. doi:10.1038/mp.2015.146.
- Dubois, B., Feldman, H.H., Jacova, C., Hampel, H., Molinuevo, J.L., Blennow, K., DeKosky, S.T., Gauthier, S., Selkoe, D., Bateman, R., Cappa, S., Crutch, S., Engelborghs, S., Frisoni, G.B., Fox, N.C., Galasko, D., Habert, M.O., Jicha, G.A., Nordberg, A., Pasquier, F., Rabinovici, G., Robert, P., Rowe, C., Salloway, S., Sarazin, M., Epelbaum, S., de Souza, L.C., Vellas, B., Visser, P.J., Schneider, L., Stern, Y., Scheltens, P., Cummings, J.L. 2014. Advancing research diagnostic criteria for Alzheimer's disease: the IWG-2 criteria. *Lancet Neurol* 13(6), 614-29. doi:10.1016/S1474-4422(14)70090-0.
- Gobbi, M., Re, F., Canovi, M., Beeg, M., Gregori, M., Sesana, S., Sonnino, S., Brogioli, D., Musicanti, C., Gasco, P., Salmona, M., Masserini, M.E. 2010. Lipid-based nanoparticles with high binding affinity for amyloid-beta1-42 peptide. *Biomaterials* 31(25), 6519-29. doi:10.1016/j.biomaterials.2010.04.044.
- Hampel, H., Shen, Y., Walsh, D.M., Aisen, P., Shaw, L.M., Zetterberg, H., Trojanowski, J.Q., Blennow, K. 2010. Biological markers of amyloid beta-related mechanisms in Alzheimer's disease. *Exp Neurol* 223(2), 334-46. doi:10.1016/j.expneurol.2009.09.024.
- Hardy, J., Selkoe, D.J. 2002. The amyloid hypothesis of Alzheimer's disease: progress and problems on the road to therapeutics. *Science* 297(5580), 353-6. doi:10.1126/science.1072994.

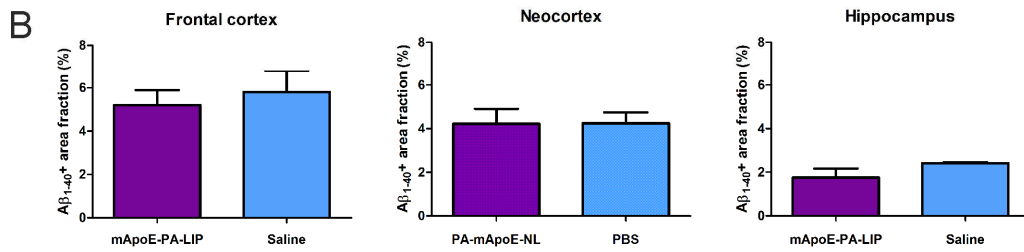
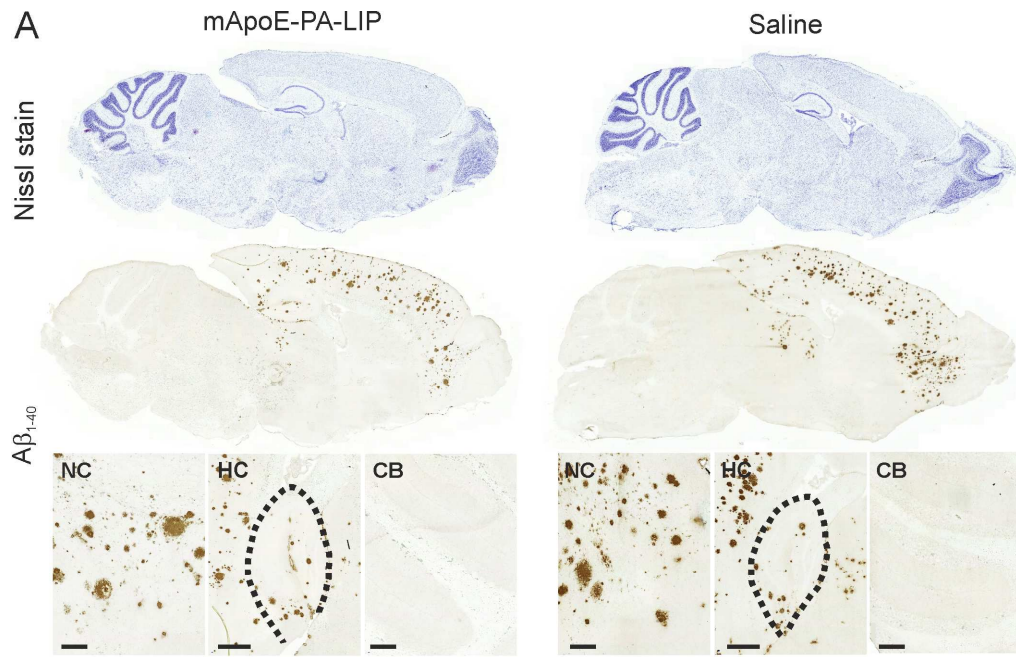
- Hardy, J.A., Higgins, G.A. 1992. Alzheimer's disease: the amyloid cascade hypothesis. *Science* 256(5054), 184-5.
- Jewett, D.M. 1992. A simple synthesis of [¹¹C]methyl triflate. *Int J Rad Appl Instrum A* 43(11), 1383-5.
- Karran, E., De Strooper, B. 2016. The amyloid cascade hypothesis: are we poised for success or failure? *J Neurochem* 139 Suppl 2, 237-52. doi:10.1111/jnc.13632.
- Karran, E., Hardy, J. 2014. A critique of the drug discovery and phase 3 clinical programs targeting the amyloid hypothesis for Alzheimer disease. *Ann Neurol* 76(2), 185-205. doi:10.1002/ana.24188.
- Klunk, W.E., Lopresti, B.J., Ikonovic, M.D., Lefterov, I.M., Koldamova, R.P., Abrahamson, E.E., Debnath, M.L., Holt, D.P., Huang, G.F., Shao, L., DeKosky, S.T., Price, J.C., Mathis, C.A. 2005. Binding of the positron emission tomography tracer Pittsburgh compound-B reflects the amount of amyloid-beta in Alzheimer's disease brain but not in transgenic mouse brain. *J Neurosci* 25(46), 10598-606. doi:25/46/10598 [pii]10.1523/JNEUROSCI.2990-05.2005.
- Larsen, P., Ulin, J., Dahlstrom, K., Jensen, M. 1997. Synthesis of ¹¹C-iodomethane by iodination of ¹¹C-methane. *Appl Radiat Isot Appl Radiat Isot* 48, 153-7.
- Maeda, J., Ji, B., Irie, T., Tomiyama, T., Maruyama, M., Okauchi, T., Staufenbiel, M., Iwata, N., Ono, M., Saido, T.C., Suzuki, K., Mori, H., Higuchi, M., Suhara, T. 2007. Longitudinal, quantitative assessment of amyloid, neuroinflammation, and anti-amyloid treatment in a living mouse model of Alzheimer's disease enabled by positron emission tomography. *J Neurosci* 27(41), 10957-68. doi:27/41/10957 [pii]10.1523/JNEUROSCI.0673-07.2007.
- Maier, F.C., Wehrl, H.F., Schmid, A.M., Mannheim, J.G., Wiehr, S., Lerdkrai, C., Calaminus, C., Stahlschmidt, A., Ye, L., Burnet, M., Stiller, D., Sabri, O., Reischl, G., Staufenbiel, M., Garaschuk, O., Jucker, M., Pichler, B.J. 2014. Longitudinal PET-MRI reveals β -amyloid deposition and rCBF dynamics and connects vascular amyloidosis to quantitative loss of perfusion. *Nat Med* 20(12), 1485-92. doi:10.1038/nm.3734.
- Mancini, S., Minniti, S., Gregori, M., Sancini, G., Cagnotto, A., Couraud, P.O., Ordonez-Gutierrez, L., Wandosell, F., Salmona, M., Re, F. 2016. The hunt for brain Abeta oligomers by peripherally circulating multi-functional nanoparticles: Potential therapeutic approach for Alzheimer disease. *Nanomedicine* 12(1), 43-52. doi:10.1016/j.nano.2015.09.003.
- Manook, A., Yousefi, B.H., Willuweit, A., Platzer, S., Reder, S., Voss, A., Huisman, M., Settles, M., Neff, F., Velden, J., Schoor, M., von der Kammer, H., Wester, H.J., Schwaiger, M., Henriksen, G., Drzezga, A. 2012. Small-Animal PET Imaging of Amyloid-Beta Plaques with [¹¹C]PiB and Its Multi-Modal Validation in an APP/PS1 Mouse Model of Alzheimer's Disease. *PLoS One* 7(3), e31310. doi:09-PONE-RA-14152 [pii]10.1371/journal.pone.0031310.
- Mouse MRI brain template. 2005. Mouse MRI brain template. MRM NAt Mouse Brain Database, McKnight Brain Institute, <http://brainatlas.mbi.ufl.edu/Database/>.
- Re, F., Cambianica, I., Sesana, S., Salvati, E., Cagnotto, A., Salmona, M., Couraud, P.O., Moghimi, S.M., Masserini, M., Sancini, G. 2010. Functionalization with ApoE-derived peptides enhances the interaction with brain capillary endothelial cells of nanoliposomes binding amyloid-beta peptide. *J Biotechnol* 156(4), 341-6. doi:10.1016/j.jbiotec.2011.06.037.
- Re, F., Cambianica, I., Zona, C., Sesana, S., Gregori, M., Rigolio, R., La Ferla, B., Nicotra, F., Forloni, G., Cagnotto, A., Salmona, M., Masserini, M., Sancini, G. 2011. Functionalization of liposomes with ApoE-derived peptides at different density affects cellular uptake and drug

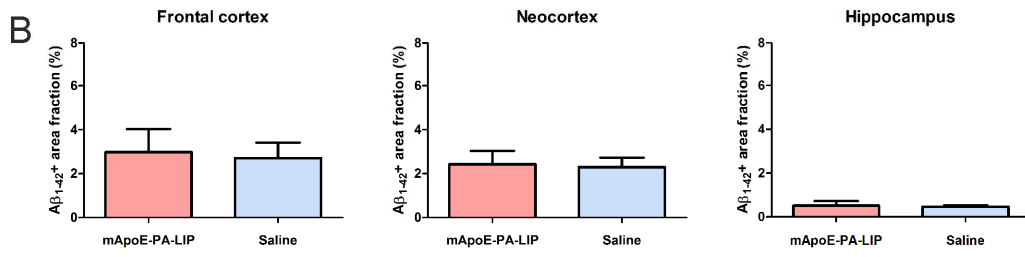
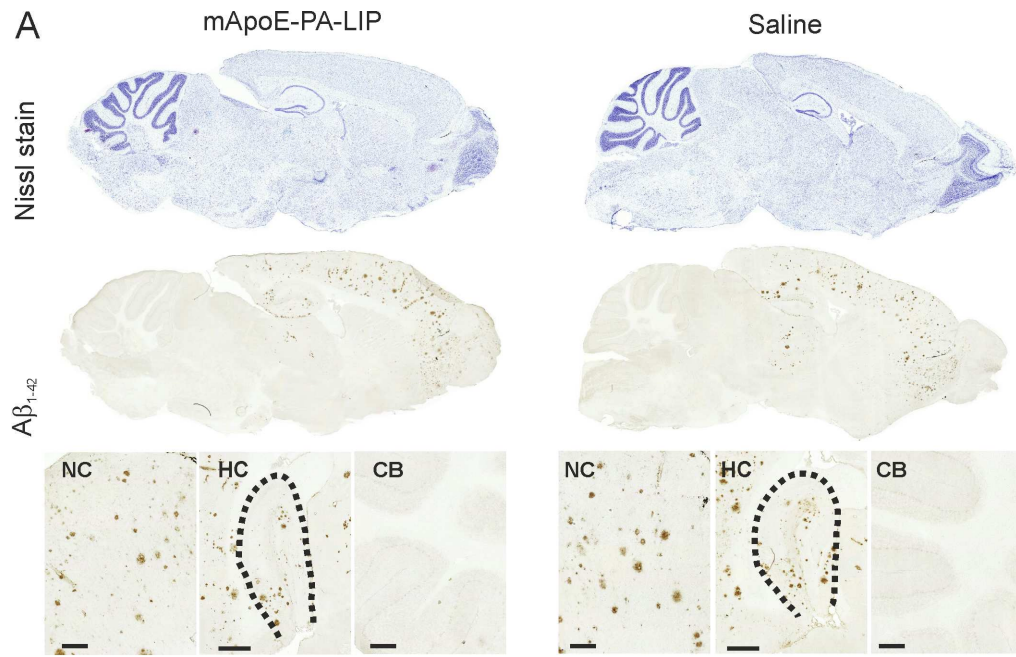
- transport across a blood-brain barrier model. *Nanomedicine* 7(5), 551-9. doi:10.1016/j.nano.2011.05.004.
- Re, F., Gregori, M., Masserini, M. 2012. Nanotechnology for neurodegenerative disorders. *Nanomedicine* 8 Suppl 1, S51-8. doi:10.1016/j.nano.2012.05.007.
- Rominger, A., Brendel, M., Burgold, S., Keppler, K., Baumann, K., Xiong, G., Mille, E., Gildehaus, F.J., Carlsen, J., Schlichtiger, J., Niedermoser, S., Wängler, B., Cumming, P., Steiner, H., Herms, J., Haass, C., Bartenstein, P. 2013. Longitudinal assessment of cerebral β -amyloid deposition in mice overexpressing Swedish mutant β -amyloid precursor protein using 18F-florbetaben PET. *J Nucl Med* 54(7), 1127-34. doi:10.2967/jnumed.112.114660.
- Snellman, A., López-Picón, F.R., Rokka, J., Salmons, M., Forloni, G., Scheinin, M., Solin, O., Rinne, J.O., Haaparanta-Solin, M. 2013. Longitudinal amyloid imaging in mouse brain with 11C-PIB: comparison of APP23, Tg2576, and APPsw-PS1dE9 mouse models of Alzheimer disease. *J Nucl Med* 54(8), 1434-41. doi:10.2967/jnumed.112.110163.
- Snellman, A., Rokka, J., Lopez-Picon, F.R., Eskola, O., Wilson, I., Farrar, G., Scheinin, M., Solin, O., Rinne, J.O., Haaparanta-Solin, M. 2012. Pharmacokinetics of [(18)F]flutemetamol in wild-type rodents and its binding to beta amyloid deposits in a mouse model of Alzheimer's disease. *Eur J Nucl Med Mol Imaging* 39(11), 1784-95. doi:10.1007/s00259-012-2178-9.
- Snellman, A., Rokka, J., López Picón, F.R., Eskola, O., Salmons, M., Forloni, G., Scheinin, M., Solin, O., Rinne, J.O., Haaparanta-Solin, M. 2014. In vivo PET imaging of beta-amyloid deposition in mouse models of Alzheimer's disease with a high specific activity PET imaging agent [18F]flutemetamol. *EJNMMI Research* 4(37). doi:10.1186/s13550-014-0037-3.
- Sturchler-Pierrat, C., Abramowski, D., Duke, M., Wiederhold, K.H., Mistl, C., Rothacher, S., Ledermann, B., Bürki, K., Frey, P., Paganetti, P.A., Waridel, C., Calhoun, M.E., Jucker, M., Probst, A., Staufenbiel, M., Sommer, B. 1997. Two amyloid precursor protein transgenic mouse models with Alzheimer disease-like pathology. *Proc Natl Acad Sci U S A* 94(24), 13287-92.
- Sturchler-Pierrat, C., Staufenbiel, M. 2000. Pathogenic mechanisms of Alzheimer's disease analyzed in the APP23 transgenic mouse model. *Ann N Y Acad Sci* 920, 134-9.
- Sérrière, S., Tauber, C., Vercouillie, J., Mothes, C., Pruckner, C., Guilloteau, D., Kassiou, M., Doméné, A., Garreau, L., Page, G., Chalon, S. 2015. Amyloid load and translocator protein 18 kDa in APPswPS1-dE9 mice: a longitudinal study. *Neurobiol Aging*. doi:10.1016/j.neurobiolaging.2014.11.023.
- Wimo, A., Ballard, C., Brayne, C., Gauthier, S., Handels, R., Jones, R.W., Jonsson, L., Khachaturian, A.S., Kramberger, M. 2014. Health economic evaluation of treatments for Alzheimer's disease: impact of new diagnostic criteria. *J Intern Med* 275(3), 304-16. doi:10.1111/joim.12167.
- Zimmer, E.R., Parent, M.J., Cuellar, A.C., Gauthier, S., Rosa-Neto, P. 2014. MicroPET imaging and transgenic models: a blueprint for Alzheimer's disease clinical research. *Trends Neurosci* 37(11), 629-41. doi:10.1016/j.tins.2014.07.002.

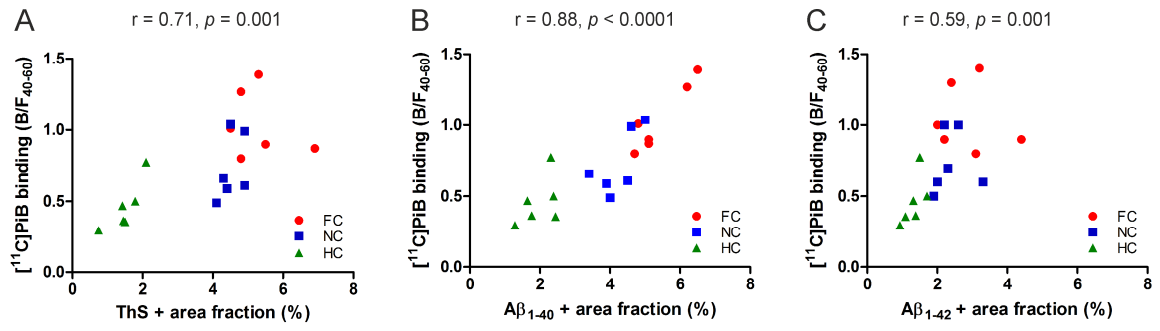












Usability of [¹¹C]PIB micro-PET imaging for *in vivo* follow-up of anti-amyloid treatment effects in APP23 mouse model

Anniina Snellman^{a,b,c*}, Johanna Rokka^d, Francisco R. Lopez-Picon^{a,b}, Semi Helin^d, Francesca Re^e, Eliisa Löyttyniemi^f, Rea Pihlaja^{a,b}, Gianluigi Forloni^g, Mario Salmona^g, Massimo Masserini^e, Olof Solin^{d,h,i}, Juha O. Rinne^j, Merja Haaparanta-Solin^{a,b}

Highlights

- Functionalized A β -targeted liposomes were administrated to transgenic APP23 mice
- Longitudinal changes in A β deposition were followed *in vivo* with micro-PET imaging
- Significant correlation was found between [¹¹C]PIB binding and brain A β load
- The results support animal stratification based on the baseline data
- The results support normalization of treatment effects to baseline values